PROCEEDINGS OF SCIENCE

Signature of adiabatic expansion in the Radio-γ-ray response of blazars

Andrea Tramacere,[a,*] **Vitalii Sliusar ,**[a] **Rolad Walter ,**[a] **Jakub Jurysek** [a,b] **and Matteo Balbo**[a]

[a] *Department of Astronomy, University of Geneva, Chemin Pegasi 51, CH-1290 Versoix, Switzerland*

[b] *FZU - Institute of Physics of the Czech Academy of Sciences, Na Slovance 1999/2, 182 21 Praha 8, Czech Republic*

E-mail: andrea.tramacere@unige.ch

Long-term campaigns for several blazars show that the radio emission occurs with a significant delay with respect to the γ-ray band, with timescales ranging from weeks to years. This observational evidence has long been a matter of debate and is usually interpreted as a signature of the γ-ray emission originating upstream in the jet, with the emitting region becoming radio transparent at larger scales. In the presented analysis we show, by means of self-consistent numerical modelling, that a relativistic blob, undergoing an adiabatic expansion, can explain these delays, reproducing lags compatible with the observed timescales. We use the JetSeT framework to reproduce the numerical modelling of the radiative and accelerative processes, reproducing the temporal evolution of a single blob, from the initial flaring activity and the subsequent expansion, following the spectral evolution and the corresponding light curves, investigating the relations among the observed parameters, rise time, delay, and decay time, and we identify the link with physical parameters. We find that, when adiabatic expansion is active, lags due to the shift of the synchrotron frequency occur. The delay, rising, and decaying timescales depends on the velocity of the expansion and on the time required for the source to exhibit an SSA frequency below the observed radio frequency. We derive an inter-band response function, embedding the parameters mentioned above, and we investigate the effects of the competition between radiative and adiabatic cooling timescales on the response. We apply the response function to long-term radio and γ-ray light curves of Mrk 421, finding satisfactory agreement on the long-term behaviour, and we use a Monte Carlo Markov Chain approach to estimate some relevant physical parameters.

7th Heidelberg International Symposium on High-Energy Gamma-Ray Astronomy (Gamma2022)
4-8 July 2022
Barcelona, Spain

*Speaker

PoS(Gamma2022)099

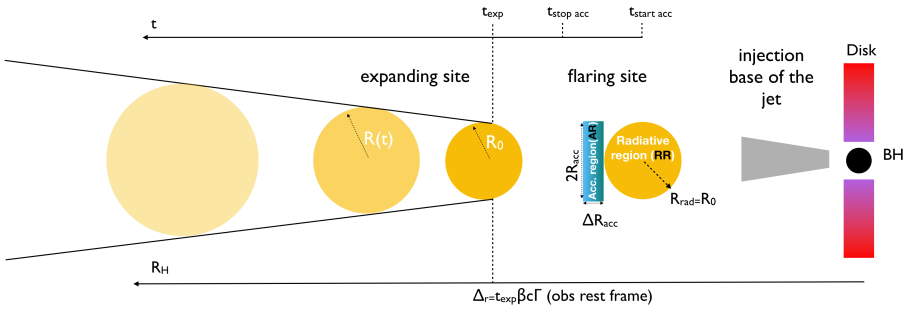

Figure 1: Schematic representation of the model implemented in `JetSeT`. At time $t_{\text{start acc}}$, particles are injected and accelerated in the acceleration region where they undergo both cooling and acceleration processes and diffuse towards the radiative region, where only losses take place. The acceleration process ends at time $t_{\text{stop acc}}$. After a time t_{exp}, the expansion process takes place in the RR region. Figure adapted from [16].

1. Introduction

Long-term multiwavelength campaigns for several blazars have shown radio emission occurring with a significant delay with respect to the γ-ray band, with timescales ranging from weeks to years [6, 9]. This observational evidence is not compatible with different cooling timescales, and has been a matter of debate for several years. A possible interpretation was proposed by taking into account the different distances of the $\gamma-$ray and radio transparent region, with the moving region becoming transparent to the γ-rays [4] and later to the radio frequencies [3]. A key aspect to investigate in this scenario is to understand the role of the adiabatic expansion of the emitting region, and the consequences in terms of variation of the synchrotron self-absorption frequency (SSA), as presented in the seminal works by [7] and [18] and more recently, [8], [5] and [16]. In this paper, we report a summary of the most significant results presented in [16], based on the self-consistent numerical modelling of the adiabatic expansion of a relativistic blob, and the derivation of an inter-band response function, embedding the physical parameters of the model.

2. Model description for adiabatic expansion.

To follow the evolution of the emitting particle distribution, and the radiative fields, we use the `JetTimeEvol` class from the `jet_timedep` module of the open-source `JetSeT`[1] framework [13–15]. This class allows the user to evolve the particle distribution under the effects of radiative cooling, adiabatic expansion, and acceleration processes (both systematic and stochastic), and to extract SEDs and light curves at any given time. The code proceeds through the numerical solution of a kinetic equation, following the same approach as in [15].

We set up our simulation in order to reproduce an initial flaring stage (FS), and a following expansion process happening during the long-term stage (LTS), within a leptonic synchrotron self-Compton (SSC) scenario. During the flare, particles are injected and accelerated in the acceleration region (AR) where they undergo both cooling and acceleration processes, and diffuse toward the radiative region (RR), where only losses take place (here after, all the quantities are expressed in the frame of the emitting blob, except for those labelled with the *obs* flag). After a time t_{exp}, the expansion process takes place in the RR region. We follow the LTS evolution under the effects of radiative cooling and adiabatic expansion, setting the duration of the simulation

[1] https://github.com/andreatramacere/jetset

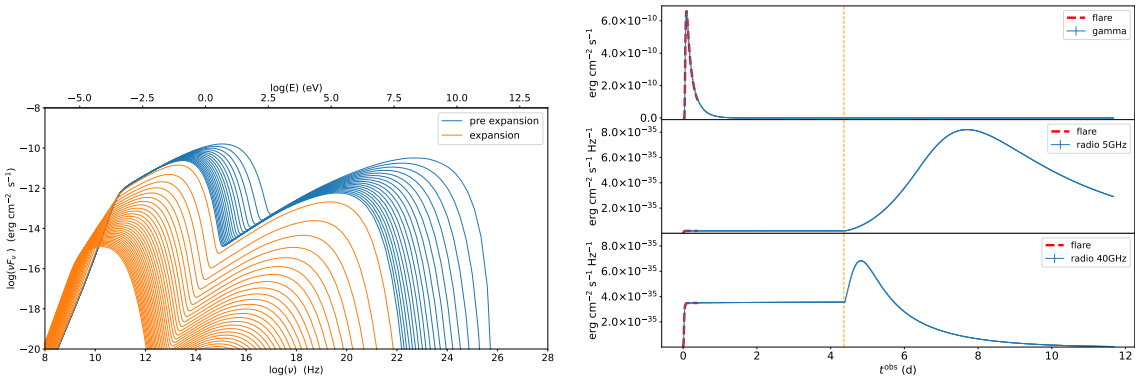

Figure 2: Simulation of an expansion episode, for $\beta_{\rm exp} = 0.1$. The *left panel* shows the evolution of the SEDs for the LTS, where the blue colour indicates to the pre-expansion stage, and orange indicates the expansion stage. The *right* panels show the merged light curves (FS and LTS) in the Fermi-LAT band, and at 5 and 40 GHz. The red dashed lines mark the light-curve segment belonging to the FS and the orange vertical dashed lines mark the beginning of the expansion in the LTS. An animated version of this simulation can be found on YouTube. Figure adapted from [16].

to be long enough to follow the particle evolution due to the expansion process. A schematic representation of these processes is shown in Figure 1. A detailed description of the model is reported in [16]. The values of the magnetic field (B) and the radius (R) in the RR during the flaring episode are taken from the typical values derived from MW modelling for HBLs, and these values coincide with the initial values at the beginning of the expansion (B_0 and R_0). Hence, we only extrapolate the evolution of $B(t) = B_0\left(\frac{R_0}{R(t)}\right)^{m_B}$, (dictated by flux freezing [2]) according to m_B and $R(t) = R_0 + \beta_{\rm exp} c(t - t_{\rm exp})H(t - t_{\rm exp})$, from the beginning of the expansion process, assuming that the expansion begins at a time $t_{\rm exp}$, with a constant expansion velocity $\beta_{\rm exp} = v_{\rm exp}/c$, and that the particles are confined within the RR. Light curves are obtained by integrating SEDs between two frequencies, or as monochromatic.

3. Radio-γ response and phenomenological relations

In Figure 2 we show an example of expansion for the value of $\beta_{\rm exp} = 0.1$ and $t_{\rm exp} = 1 \times 10^7$ s. The evolution of the SEDs, for the post-flare non-expanding stage (left panel, blue lines), follows the usual pattern dictated by the radiative cooling timescales, whilst during the expanding-stage (orange lines) the evolution pattern changes. The most interesting effect is the evolution of the S component. On top of the flux decay dictated by the adiabatic losses and decreased magnetic field, we notice the shift in the SSA frequency, which is absent in the non-expanding stage. Whilst during the non-expanding stage the SSA is almost stable at the initial value of $\approx 10^{11}$ Hz, in the expanding stage, the SSA decreases with time according to $\nu^*_{\rm SSA}(t) = \nu^0_{\rm SSA}\left[\frac{R(t)}{R_0}\right]^{\phi}$ [16], where $\nu^0_{\rm SSA}$ is the SSA before the expanding stage, and p is the low-energy power-law index of the emitting electron distribution, and $\phi = \frac{p+4}{m_B(p+2)+4}$. The three right panels show the light curves in the Fermi-LAT band, and at 5 and 40 GHz. For the case of the lightcurve, we show also the flaring episode (red dashed lines). During the post-flare non-expanding stage, the temporal behaviour is again in agreement with a purely radiative cooling without particle escape. On the contrary, in the expanding stage, the radio light curves increases in flux level when the expansion starts, with the time of the maximum happening earlier at larger frequencies (an animated version of this simulation can be found on YouTube). The delays and the different rise and decay times can be quantified using

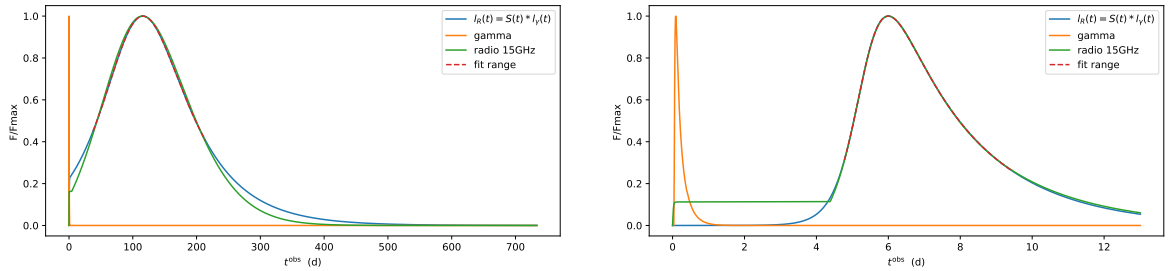

Figure 3: Convolution response, for two numerical simulations with the same parameters as in Figure 2, except$\beta_{exp} = 0.001$ (*left panel*) and $\beta_{exp} = 0.08$ (*right panel*). The red dashed line represents the actual fit interval, the orange line represents the γ-ray light curve in, the green line the 15 GHz radio light curve, and the blue line is the best fit of the radio light curve obtained from the convolution of the γ-ray light curve with the best-fit response. Figure adapted from [16].

the phenomenological trends derived and validated in [16](). These trends, in the observer, as a function of the observed SSA in the expanding stage, $\nu^{*,obs}_{SSA}$, reads:

$$
\begin{aligned}
t^{obs}_{decay} &= \frac{R^{obs}_0}{m_B \beta_{exp} c}\left(\frac{\nu^{0,obs}_{SSA}}{\nu^{*,obs}_{SSA}}\right)^{\phi} \\
t^{obs}_{rise} &= \frac{1}{2}t^{obs}_{peak} = \begin{cases} \frac{1}{2}\frac{R^{obs}_0}{\beta_{exp} c}\left[\left(\frac{\nu^{0,obs}_{SSA}}{\nu^{*,obs}_{SSA}}\right)^{\phi} - 1\right] & \text{if } \nu^{0,obs}_{SSA} > \nu^{*,obs}_{SSA} \\ 0 & \text{otherwise} \end{cases} \\
\Delta t^{obs} &= t^{obs}_{exp} + t^{obs}_{peak} = t^{obs}_{exp} + \frac{R^{obs}_0}{\beta_{exp} c}\left[\left(\frac{\nu^{0,obs}_{SSA}}{\nu^{*,obs}_{SSA}}\right)^{\phi} - 1\right].
\end{aligned}
\tag{1}
$$

The radio light curves (l_R) can be reproduced as a convolution 'response' of the γ-ray light curves (l_γ) [11, 12, 17] according to $l_R(t) = S(t) * l_\gamma(t)$, where the S is an empirical function depending on parameters that can be related to the observable quantities in Equation1. The response function proposed in [16] reads: $S(t) = A\frac{\exp\frac{-(t-\Delta t)}{t_f}}{1+\exp\frac{-(t-\Delta t)}{t_u}}$, where t_f is the decay time, and t_u is the rise time. This is the combination of a logistic function and an exponential decay, with A being a scaling factor, depending mainly on the initial value of the Compton dominance, on the observed radio frequency, and on m_B. The actual determination of the delay, rise and decay time as function of t^{obs}_{decay}, t^{obs}_{rise}, and Δt^{obs} is derived in [16]. In Figure 3 we show an example of response application, to the 15 GHz radio lightcurve, for the two numerical simulations with the same parameters as in Figure 2, except $\beta_{exp} = 0.001$ (*left panel*) and $\beta_{exp} = 0.08$ (*right panel*). The value of β_{exp} impacts on t^{obs}_{decay}, t^{obs}_{rise} and Δt^{obs}, according to the trends in Equation 1.

4. Application of the radio-γ response to observational data for Mrk 421.

We applied the response and the phenomenological trends discussed above to real data from *Fermi*-LAT [1] (in the 1-300 GeV band) and from the OVRO radio telescope [10] for Mrk 421 (see [16] for details on Fermi-LAT lightcurve extraction). In the left panel of Figure 4 we show the reads of best-fit response obtained by minimising, over a 7.5-year period (MJD 55500-58226), the deviations between the observed radio light curve and the synthetic light curve obtained by the convolution of the Fermi LAT daily binned light curve with the response $S(t)$, discussed above.

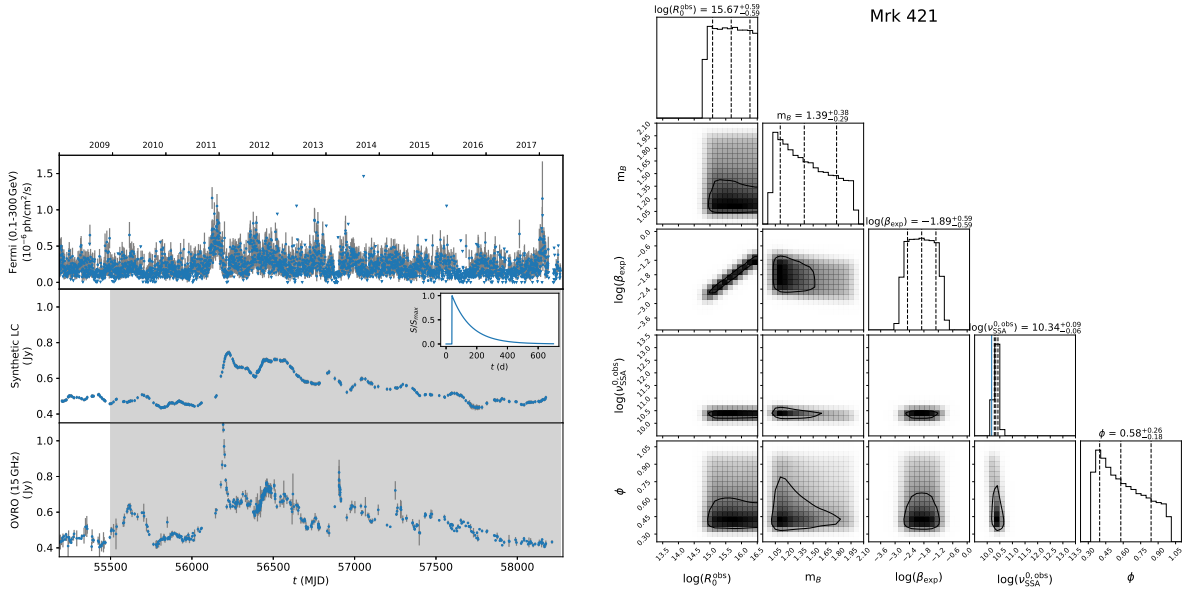

Figure 4: *Left panel:* synthetic radio light curve for Mrk 421 (middle) created as a convolution of the day-binned Fermi-LAT 0.1-300 GeV light curve (top) and of the radio response (inset panel), compared with the OVRO 15 GHz radio light curve (bottom). Fitting time range is highlighted in grey. *Right panel:* posterior distribution for a MCMC sampling of the composite log-likelihood for rise, decay, and delay time in Equation 1. To sample the parameter space, we use uninformative flat priors, with $m_B \in [1, 2]$, $\phi \in [1/3, 1]$, $\nu^{0,\mathrm{obs}}_{\mathrm{SSA}} \in [10, 10^4]$ GHz, $\beta_{\mathrm{exp}} \in [10^{-4}, 1]$. The range of R^{obs}_0 is determined by setting a flat range for the observed γ-ray variability timescale $t^{\mathrm{var}}_\gamma \in [0.25, 14]$ days, and setting $R^{\mathrm{obs}}_0 = t^{\mathrm{var}}_\gamma c$, corresponding to $R^{\mathrm{obs}}_0 \in [6.5 \times 10^{13}, 3.6 \times 10^{17}]$ cm. The solid black identifies the 1-σ containment for a bivariate Gaussian distribution. On the diagonal, we plot the marginalised posterior distributions, and with the vertical dashed black lines we indicate the 0.16, 0.5, and 0.84 quantiles. The blue vertical line in the $\log(\nu^{0,\mathrm{obs}}_{\mathrm{SSA}})$ histogram identifies the 15 GHz observed OVRO frequency. On top of each marginalised histogram we report the confidence level corresponding to the quantiles. Figure adapted from [16].

The Fermi LAT light curve starts about two years before the period used for the minimisation to account for the long-lasting effect of the response, particularly Δt^{obs}. The observed GeV and radio and the resulting synthetic radio light curves are shown in the top panel of Figure 4, and resulted in a $\Delta t^{\mathrm{obs}} = 37.58^{+0.13}_{-0.13}$, $t^{\mathrm{obs}}_{\mathrm{rise}} =\lesssim 1$ day, and $t^{\mathrm{obs}}_{\mathrm{decay}} = 126.5^{+1.3}_{-1.3}$ days. The synthetic light curve reproduces the long-term trend, with short-term deviations possibly hinting for a change in the intensity of the response (e.g. the non-constant A, or a change in the beaming factor due to a bending jet), or possible different origin of single flares, as for the case of the fast radio flare near MJD 56897 and a wider flare at about MJD 55600 (see Figure 4). As the response rise time is similar to the binning time of the GeV light curve, its value indicates a rising time of shorter than one day.

A deeper understanding of the physics embedded in the convolution analysis, was achieved using a Monte Carlo Markov Chain (MCMC) approach, defining a composite log-likelihood $\mathcal{L} = \mathcal{L}_{\mathrm{rise}} + \mathcal{L}_{\mathrm{decay}} + \mathcal{L}_{\mathrm{delay}}$, where $\mathcal{L}_{\mathrm{rise}}$, $\mathcal{L}_{\mathrm{decay}}$, and $\mathcal{L}_{\mathrm{delay}}$ represent the log-likelihood functions corresponding to rise, decay, and delay time in Equation 1 (see [16] for more details). The results are shown in the right panel of Figure 4. The sampler provides informative confidence regions for the parameters of interest, except for $\log(R_0)$ where we notice a flat posterior for $\log(R^{\mathrm{obs}}_0) = 15.67^{+0.59}_{-0.59}$. The magnetic index $m_B = 1.39^{+0.38}_{-0.29}$ has the peak of the PDF at $m_B = 1$. The low value of $\log(\nu^{0,\mathrm{obs}}_{\mathrm{SSA}})$, corresponding to $\nu^{0,\mathrm{obs}}_{\mathrm{SSA}} \approx 22$ GHz, si compatible with by the short $t^{\mathrm{obs}}_{\mathrm{rise}}$ returned by the convolution analysis, and very close the observed OVRO frequency of 15 GHz.

The posterior confidence level of the index ϕ implies $p = 1.97^{+1.26}_{-0.72}$, a value compatible with the predictions from Fermi first-order acceleration plus a stochastic component, which is in agreement with previous theoretical and observational analyses [14, 15].

5. Conclusions

We reported a summary of the most significant results presented in [16]. When adiabatic expansion is active, delays between radio and $\gamma-$ray emission, due to the shift of the SSA frequency, occur with the delay, rising, and decaying timescales depending on the velocity of the expansion and on the time required for the source to exhibit an SSA frequency below the observed radio frequency. An inter-band response function, embedding the aforementioned parameters, applied to radio and $\gamma-$ray light curves of Mrk 421 provided a satisfactory agreement on the log-term variability, and by using a MCMC sampler we were able to estimate some relevant physical parameters of the jet. Future developments of the presented analysis to polarization measurements and to jet collimation profile kinematics, can provide a useful tool to investigate how relativistic jets in blazars form and develop, to understand the transition from the kinematically to the magnetically dominated regime, and, possibly, to identify extra variability patterns due, for example, to a bending jet, and the connection with the localization of the high-energy flaring site, where the particle acceleration occurs. The work presented here is fully reproducible by following the instructions in the git repository[2], and a detailed description of the analysis can be found in the JetSeT YouTube channel.

References

[1] Atwood W. B., et al., 2009, ApJ, 697, 1071
[2] Begelman M. C., Blandford R. D., Rees M. J., 1984, Rev. Mod. Phys., 56, 255
[3] Blandford R. D., Königl A., 1979, ApJ, 232, 34
[4] Blandford R. D., Levinson A., 1995, ApJ, 441, 79
[5] Boula, S. Mastichiadis, A. 2022, A&A, 657, A20
[6] Max-Moerbeck W., et al., 2014, MNRAS, 445, 428
[7] McCray R., 1969, ApJ, 156, 329
[8] Potter W. J., 2018, MNRAS, 473, 4107
[9] Pushkarev A. B., Kovalev Y. Y., Lister M. L., 2010, ApJ, 722, L7
[10] Richards J. L., et al., 2011, ApJS, 194, 29
[11] Sliusar V., et al., 2019a, in High Energy Phenomena in Relativistic Outflows VII. p. 32 (arXiv:1909.13106)
[12] Sliusar V., et al., 2019b, in 36th International Cosmic Ray Conference (ICRC2019). p. 796 (arXiv:1908.09770)
[13] Tramacere A., 2020, JetSeT: Numerical modeling and SED fitting tool for relativistic jets (ascl:2009.001)
[14] Tramacere A., Giommi P., Perri M., Verrecchia F., Tosti G., 2009, A&A, 501, 879
[15] Tramacere A., Massaro E., Taylor A. M., 2011, The Astrophysical Journal, 739, 66
[16] Tramacere A., Sliusar V., Walter R., Jurysek J., Balbo M., 2022, A&A, 658, A173
[17] Türler M., Courvoisier T. J.-L., Paltani S., 1999, A&A, 349, 45
[18] van der Laan H., 1969, in Quasars and high-energy astronomy. p. 49

[2] https://github.com/andreatramacere/adiabatic_exp_radio_gamma_delay